LAWRENCE
LIVERMORE
NATIONAL
LABORATORY

LLNL-JRNL-516876

Development and calibration of mirrors and gratings for the Soft X-Ray Materials Science beamline at the LCLS free-electron laser

R. Soufli, E. T. Al

November 29, 2011

Applied Optics

Disclaimer

Development and calibration of mirrors and gratings for the Soft X-Ray Materials Science beamline at the LCLS free-electron laser

Regina Soufli[1], Mónica Fernández-Perea[1,2], Sherry L. Baker[1], Jeff C. Robinson[1], Eric M. Gullikson[3], Philip Heimann[3,4], Valeriy V. Yashchuk[3], Wayne R. McKinney[3], William F. Schlotter[4] and Michael Rowen[4]

[1]Lawrence Livermore National Laboratory, 7000 East Avenue, Livermore, CA 94550

[2]Consejo Superior de Investigaciones Científicas, C/ Serrano 144, 28006 Madrid, Spain

[3]Lawrence Berkeley National Laboratory, 1 Cyclotron Road, Berkeley, CA 94720

[4]SLAC National Accelerator Laboratory, 2575 Sand Hill Road, Menlo Park, CA 94025

Abstract

This work discusses the development and calibration of the x-ray reflective and diffractive elements for the Soft X-Ray Materials Science (SXR) beamline of the Linac Coherent Light Source (LCLS) free-electron laser (FEL), designed for operation in the 500 – 2,000 eV region. The surface topography of three Si mirror substrates and two Si diffraction grating substrates was examined by atomic force microscopy (AFM) and optical profilometry. The figure of the mirror substrates was also verified via surface slope measurements with a long trace profilometer. A boron carbide (B_4C) coating especially optimized for the LCLS FEL conditions was deposited on all SXR mirrors and gratings. Coating thickness uniformity of 0.14 nm root-mean-square (rms) across clear apertures extending to 205 mm length was demonstrated for all elements, as required

to preserve the coherent wavefront of the LCLS source. The reflective performance of the mirrors and the diffraction efficiency of the gratings were calibrated at beamline 6.3.2. at the Advanced Light Source synchrotron. To verify the integrity of the nanometer-scale grating structure, the grating topography was examined by AFM before and after coating. This is the first time where B_4C-coated diffraction gratings are demonstrated for operation in the soft x-ray region.

1. Introduction

The Linac Coherent Light Source (LCLS)[1] is the first x-ray free electron laser (FEL) facility in the world and began its operation in 2009 at the SLAC National Accelerator Laboratory in Menlo Park, California. This unique x-ray source produces ~100 femtosecond monochromatic X-ray pulses of extremely high brightness [10^{32} photons sec^{-1} mm^{-2} $mrad^{-2}$ (0.1% bandwidth)$^{-1}$] in the first harmonic, between 500 eV and 8 keV. The revolutionary capabilities of the LCLS are enabling groundbreaking new research in the fields of physics, biology, life sciences and materials science.

The Soft X-ray Materials Science (SXR) beamline at the LCLS provides intense, ultra-short soft x-ray pulses generated by the LCLS FEL and can accommodate experimental configurations such as x-ray emission, coherent imaging, resonant scattering, photoelectron spectroscopy and x-ray absorption spectroscopy. The scientific experiments that can be performed at the SXR beamline cover a variety of fields such as catalysis, magnetism, correlated materials, clusters and biological structure[2]. A schematic layout of the SXR beamline is shown in Fig. 1, and the main parameters for each of its optics (mirrors and gratings) are summarized in Table 1. The beamline is equipped with a monochromator, consisting of a pre-focusing mirror M1 and two varied-line

spacing (VLS) gratings G1 and G2, whose energy range (500 eV – 2,000 eV) covers several of the K- and L- edges of important materials for resonant excitation with as-designed resolving power around 5000. The SXR beamline can also deliver beam in non-monochromatic mode. Mirrors M2, M3 form a Kirkpatrick-Baez pair, which can focus the beam from about 1 mm^2 to 2 μm^2 spot size. In Endstation 1, before the monochromator, samples can be studied in transmission mode, detected in a single shot setup at the monochromator exit slit position. The optical design of the SXR beamline and its monochromator are discussed in more detail in Ref. 3.

The principles and concepts for the design and fabrication of x-ray optics for the LCLS FEL have been discussed in detail in previous literature[4,5,6,7,8]. One of the unique features of the LCLS is the extremely high instantaneous dose of the LCLS x-ray beam mentioned above, which severely limits the choice of x-ray mirror materials. Boron carbide (B_4C) was found to be among the very few materials that can survive the peak brightness of the soft x-ray LCLS FEL beam[9,10] which is higher by over 10 orders of magnitude compared to current 3rd generation synchrotron sources. In addition to its high FEL damage threshold, B_4C also has excellent reflective performance at grazing incidence angles in the 500 – 2,000 eV photon energy region where the SXR beamline operates. Another major requirement for LCLS is the preservation of the spatial coherence of the LCLS beam wavefront which translates to very stringent surface figure and finish specifications for the LCLS x-ray reflective elements. The surface specifications for the figure, mid-spatial frequency roughness (MSFR) and high-spatial frequency roughness (HSFR) of the SXR beamline mirrors and gratings are presented in Section 3. Given that bulk B_4C cannot be polished and figured to x-ray optics quality, the LCLS soft x-ray mirrors and gratings were designed to consist of a boron carbide coating deposited at Lawrence Livermore National

Laboratory (LLNL) on top of a polished silicon (Si) substrate supplied by a commercial vendor. In this manuscript, Section 2 summarizes the instruments and experimental facilities employed for the metrology, B_4C coating, and x-ray reflectance and diffraction measurements of the SXR mirrors and gratings. Section 3 discusses the Si substrate metrology and B_4C deposition results on SXR mirrors M1, M2 and M3. Section 4.1 discusses the measured topography of an SXR test grating before and after B_4C coating. Section 4.2 presents metrology, x-ray diffraction efficiency and reflectance measurements and analysis on the SXR G1 and G2 gratings.

2. Experimental setup

The surface slope and root-mean-square (rms) slope error measurements of the SXR M1, M2, and M3 mirror substrates discussed in Section 3 were performed with the long trace profiler LTP-II located at the Optical Metrology Laboratory at the Advanced Light Source (ALS) synchrotron, Lawrence Berkeley National Laboratory (LBNL). The recently upgraded ALS LTP-II has the capability to measure surface slope variation of curved optics with < 0.25 μrad rms accuracy and slightly curved and flat optics with < 0.1 μrad rms accuracy[11,12].

All Si substrates (mirrors and gratings) were cleaned at LLNL with a custom-developed process for optical surfaces. The cleaning process consists of rinsing the substrate in a water-based solution, followed by drying in a nitrogen gas environment. This process has been shown to remove polishing residue and other types of microscopic and visible contamination from the top surface[13] which, if left untreated, could compromise and even cause delamination of the subsequently deposited reflective coating. This cleaning process has been proven to preserve the surface finish of super-polished surfaces. In the case of the SXR gratings substrate, special

precautions had to be taken to ensure the nanometer-scale grating structure remained intact during the cleaning process.

The precision surface metrology discussed in Sections 3 and 4, related to the mid- and high-spatial frequencies and including metrology of the gratings was performed at LLNL. High-spatial frequencies were measured with a Digital Instruments Dimension 5000^{TM} AFM instrument equipped with an acoustic hood and vibration isolation, reaching a noise level of 0.03 nm rms. The instrument is operated in tapping mode which measures topography in air by tapping the surface with an oscillating probe tip. The probe tips were etched silicon, with a nominal tip radius of 5-10 nm. AFM scans of 1.5×1.5 μm^2, 2×2 μm^2, 5×5 μm^2 and 10×10 μm^2 areas were performed in various regions on the SXR Si mirror substrates and gratings, to determine surface roughness. AFM scans of 50×50 μm^2 and 15×15 μm^2 areas were also performed within the ruled areas of the SXR gratings, to capture the topography of the grating structure. The AFM data from each scan were stored in a 512×512 pixel array. Mid-spatial frequencies were measured using a Zygo New View^{TM} optical surface profiler. Scans were performed on the SXR Si mirror substrates with two objective lens magnifications, 2.5× and 20×, and the data from each scan were stored in a 640×480 pixel array. To determine surface roughness values, the power spectral density (PSD) was computed[14] from the height data in the AFM and Zygo scans. The PSD was formed by first calculating a two-dimensional Fourier power spectrum of the height data. Then, the spectrum was averaged azimuthally around zero spatial frequency to produce a PSD with purely radial spatial frequency dependence. This approach is valid for quasi-isotropic surfaces. The rms value σ of the HSFR or MSFR is obtained by the expression

$$\sigma^2 = \int_{f_1}^{f_2} 2\pi f S(f) df \quad , \qquad (1)$$

where f is the spatial frequency, $S(f)$ is the surface PSD, and f_1, f_2 are the lower and upper limit frequencies of the spatial frequency range relevant for HSFR and MSFR, defined in the caption of Table 3. In order to compute HSFR or MSFR in the specified spatial frequency range, a "composite" PSD often needs to be constructed, using PSD curves from different scan sizes and/or instruments. After precision surface metrology was completed, the cleaning/drying process discussed above was repeated again on each Si substrate in preparation for deposition of the B_4C reflective coating.

The B_4C coatings discussed in Section 3.2 and Section 4 were deposited using a planar DC-magnetron sputtering deposition system located at LLNL. During deposition, the substrate is mounted on a platter which passes underneath the B_4C sputtering target in a rotational motion. At the same time, the substrate is spinning around its center at several hundred rpm to average out any spatial non-uniformities of the sputtering target. In this manner, the coating thickness variation is always symmetric around the center of the substrate. An algorithm based on modulation of the rotational velocity of the deposition platter is used to control the coating thickness and to achieve the required coating thickness uniformity[15]. The base vacuum pressure in the deposition chamber was 10^{-7} Torr and argon (Ar) was used as process gas at 10^{-2} Torr, as is discussed in more detail in Section 3.2.

The x-ray reflectance, diffraction and transmission measurements discussed in this manuscript were performed at the reflectometer facility at beamline 6.3.2. of the ALS synchrotron at LBNL. The general characteristics of the reflectometer have been described in detail earlier[16,17]. The base pressure in the sample chamber is 10^{-7} Torr. The available detectors include a selection of photodiodes and a CCD camera (the latter used for sample alignment), which can be rotated 360°

around the axis of the chamber. Second harmonic and stray light suppression is achieved with an appropriate transmission filter. When third or higher-order harmonic suppression is needed, an "order suppressor" consisting of three mirrors at a variable grazing incidence angle (depending on energy range) and based on the principle of total external reflection can be used in addition to the filters. The ALS storage ring current is used to normalize the signal against the storage ring current decay. Photon energy calibration is based on the absorption edge of an appropriate filter (Si or Cr, in this work) with a relative accuracy of 0.011% rms, and can be determined with 0.007% repeatability. The reflectance results at 91.8 eV discussed in Section 3.2 were obtained with a 200 lines/mm monochromator grating, a Be filter for second-harmonic suppression and the order suppressor consisting of three carbon mirrors at 10 degrees grazing angle of incidence. Signal was collected with a Si photodiode detector with an acceptance angle of 2.4 degrees. The SXR grating diffraction efficiency measurements and x-ray reflectance measurements in the 500 to 1200 eV photon energy range discussed in Section 4.2 were obtained with a 1200 lines/mm monochromator grating. Depending on energy region, one of the following filters: Cr, Co, Cu, Mg, was used for second-harmonic and stray light suppression. To enhance the angular resolution for the grating diffraction efficiency measurements, a 0.5-mm wide horizontal slit was installed in front of the GaAsP photodiode detector, resulting in 0.12 degree angular acceptance. The filter transmission measurements discussed in Section 4.2 were obtained with a 1200 lines/mm monochromator grating and the GaAsP photodiode detector, with 1 degree angular acceptance.

3. Mirrors M1, M2 and M3

3.1 Si substrate metrology

The Si substrates for SXR mirrors M1, M2, and M3 were figured and polished by Carl Zeiss Laser Optics (Oberkochen, Germany). After delivery of the substrates, their surface slope and radius of curvature were verified by long-trace profiler measurements at LBNL using the ALS LTP-II introduced in Section 2. The measurement results are summarized in Table 2 together with figure (height) measurements provided by the substrate vendor and with the corresponding specifications. The measured slope errors represent an upper limit of the actual rms slope errors of the corresponding surfaces, because of possible contributions from residual random, systematic, and drift errors during the measurement process. Fig. 2 shows the residual slope traces of the M1, M2, and M3 substrates as measured with the LTP-II. The residual slope traces shown in Fig. 2 and the rms slope errors in Table 2 correspond to the surfaces detrended with the best fit-cylindrical shapes. For the M2 and M3 mirrors, the fitting and detrending were made over the entire clear aperture, specified in Table 1 for each mirror. For these substrates, the resulting surface figure and slope errors are well within the specification. For the M1 mirror, the measured data in Table 2 and Fig. 2(a) correspond to a surface area that is 3 mm less than the specified clear aperture. The excluded portion of the slope trace is shown in Fig. 2(a) with a dashed line. We believe that the excluded sharp slope variation is a characteristic signature of the polishing process used for fabrication of the M1 optic. Considering the reduced clear aperture, the resulting surface figure and slope errors of the M1 substrate are also well within the specification. The radii of curvature of the best fit-cylindrical surfaces detrended for the M1, M2 and M3 mirror substrates are also presented in Table 2.

Upon delivery to LLNL, the substrates were inspected, cleaned and the MSFR and HSFR properties were verified using AFM and optical profilometry measurements as is explained in Section 2. HSFR was computed according to eq. (1) using a “composite” PSD curve, made by

combining PSD curves from 10×10 μm^2 and 2×2 μm^2 AFM scans. MSFR was computed according to eq. (1) by combining PSD curves from 2.5× and 20× optical profilometer magnifications and 10×10 μm^2 AFM scans. Two locations within the clear aperture were measured on each of the M1, M2 and M3 mirror substrates, and the results demonstrated that the finish is rather uniform among all locations. The composite PSD curves obtained in this manner (averaged between the 2 locations measured on each substrate) in the HSFR and MSFR range are plotted in Fig. 3 and the corresponding rms HSFR and MSFR values are listed in Table 3. Each of the M1, M2 and M3 substrates appears to be well within specifications. It should be noted that, due to geometrical constraints related to the large thickness of the M1 substrate (see Table 1) it was not possible to obtain measurements at 2.5× magnification with the Zygo New View™ optical surface profiler. Instead, an extrapolation was used for the M1 substrate PSD in the spatial frequency range 10^{-6} – 6.6 × 10^{-6} nm^{-1}. The extrapolation was based on the measured PSD at 2.5× magnification from SXR substrate M2, which was polished by the same vendor.

3.2 B_4C coatings

The thickness of the B_4C coatings for the SXR beamline optics was specified in the range 30-40 nm, to achieve the desired reflective properties in the photon energy region of operation, while minimizing figure deformation due to coating stress and thickness errors. The B_4C coating thickness deposited on the SXR mirrors was 37.4 nm. Detailed studies on the reflectivity, stress, roughness, and composition of the B_4C coatings for the LCLS have been presented in earlier papers[5,18,19]. Briefly, the argon working pressure during B_4C deposition was 10^{-2} Torr, (increased from 10^{-3} Torr, the nominal working pressure for the LLNL deposition system), to relax the high compressive stress of these coatings from -2 GPa to about -1 GPa. The intrinsic HSFR of 37.4-

nm-thick B_4C coatings made in this manner was found to be about 0.4 nm rms as measured by AFM, when deposited on substrates with significantly lower (~ 0.05 nm rms) roughness. The MSFR of the B_4C coating replicates exactly the MSFR of the substrate, as predicted by theory and demonstrated experimentally[5]. It was not possible to measure the reflectance of the B_4C-coated M1, M2, or M3 mirrors, due to size limitations of the beamline 6.3.2 reflectometer. Instead, the x-ray reflectance of the un-ruled portion of the SXR gratings substrates was measured after B_4C coating and is presented later in Section 4.2.

The B_4C coating thickness variation is crucial to SXR mirror performance since it affects the coherent wavefront preservation of the LCLS FEL beam, discussed in Section 1. The coating thickness variation should not significantly contribute to degradation of the mirror figure. Given that the figure errors of the mirror substrate and reflective B_4C coating are uncorrelated and thus add in a quadratic fashion, the thickness variation of the B_4C film should be less than half of the substrate figure error specification, i.e: < 1 nm rms across each mirror clear aperture. In order to optimize the B_4C coating towards meeting the < 1 nm rms thickness variation requirement, a Si test substrate assembly with identical dimensions to each mirror was used. A few B_4C coating iterations were performed on the test substrates to optimize the velocity modulation parameters during deposition, until the < 1 nm rms coating thickness uniformity requirement was met. Coating uniformity was determined by fitting Kiessig interference fringes of reflectance vs. grazing incidence angle measurements at 91.8 eV performed at ALS beamline 6.3.2. Results of the final test iteration for the M1 mirror coating are shown in Fig. 4. The B_4C coating thickness was verified at 4 locations within the mirror clear aperture, including the edge locations. The B_4C coating thickness on all measured locations was found to be 37.4 $\pm$ 0.2 nm, where $\pm$ 0.2 nm is the sensitivity of the fitting method. Therefore, the B_4C thickness variation determined in this

fashion is < 0.4 nm peak-to-valley (P-V) or < 0.14 nm rms across the 205 mm-long clear aperture of the M1 mirror, well within the 1 nm rms specification. The same uniformity results were obtained for the M2 and M3 mirrors as well.

4. Diffraction gratings

4.1 Test grating

Prior to working with the actual SXR gratings, a test grating was used to verify the grating topography and performance before and after the substrate cleaning process discussed in Section 2, and after coating with the B_4C reflective coating discussed in Section 3.2. The test grating consisted of a 30-mm diameter, 10-mm thickness Si substrate polished by Carl Zeiss Laser Optics (Oberkochen, Germany). The ruling was performed by Shimadzu Corporation (Japan) using a holographic exposure method combined with an ion-beam etching method. The same vendor and methods were used for the actual SXR gratings discussed in Section 4.2. The test grating was laminar-type with 100 lines/mm ruling (constant line spacing), with a nominal 28 ± 5 nm groove depth and 2.8 μm line width. These are the nominal parameters specified at the center of the SXR grating G1, as is shown in Table 1. Fig. 5 shows 3-dimensional, 50×50 μm^2 AFM images and selected 1-dimensional line scans from these images, obtained on the test grating (i) as-received from the manufacturer, (ii) after cleaning and (iii) after coating with a 37.4 nm – thick B_4C coating. The software used to extract and analyze the 3-dimensional AFM images is described in Ref. 20.

In Fig. 5 (i), a sinusoidal-like "modulation" pattern parallel to the direction of the grating lines appears in the AFM image of the grating surface as-received. This modulation has ~ 1-1.5 μm period and ~ 1 nm peak-to-valley amplitude and is most pronounced in the area of the grooves, but also extends to the top of the lines. It is likely an artifact of the laser holographic process that

was used in the manufacture of the grating. In the 50×50 μm^{2}AFM image of the as-received grating in Fig. 5 (i), a dense population of features shaped like spikes is evident in the area of the grooves, with heights up to about 20 nm. A detail from these features is also shown in the 2×2 μm^2 AFM image in Fig. 6 (i) obtained in a groove area. These features could be attributed to some type of residue from the grating fabrication process or artifact from the ion-beam etching process that was part of the grating fabrication. In Fig. 5 (ii), after cleaning, the number of the spike features within the grating grooves appears to have been reduced and the amplitude of the modulation-like features is also slightly reduced. Fig. 6 (iii) is a 2×2 μm^2 AFM image from the top of a grating line after cleaning, and again some type of residue from the grating fabrication process is apparent in this image. Fig. 6 (ii), (iv) shows AFM images from the groove and line areas respectively, after B_4C-coating. The evolution of surface morphology and roughness after B_4C coating is consistent with earlier studies in References 5 and 18. Table 3 summarizes measured HSFR values on various locations and cleaning/coating stages of the test grating, determined from AFM measurements using the methodology in Section 3.1. On the as-received test grating, groove areas appear to have overall higher HSFR than line areas. After cleaning, the roughness of both grooves and lines appears to improve, in accord with the earlier observations in Fig. 5.

4.2 Gratings G1, G2.

Both gratings G1 (100 lines/mm) and G2 (200 lines/mm) were ruled on the same 220 × 50 mm^2 Si substrate. Each ruling was 140×10 mm^2, with G1 starting at about 8 mm from the edge of the substrate (tangential direction) and G2 immediately next to G1. The nominal groove profile parameters for each grating are summarized in Table 1. The gratings were cleaned and examined

by AFM microscopy, with similar results and observations as discussed in Section 4.1 for the test grating.

Fig. 7 shows 15×15 μm^2 and 50×50 μm^2 AFM images of the G2 (200 lines/mm) grating, as-received and after cleaning. In the 15×15 μm^2 images, there is evidence of contamination that is removed after the cleaning process. Sinusoidal-like modulation features are also apparent across the lines and grooves of grating G2, similar to those observed on the test grating in Section 4.1. The grating surface topography after deposition of the 37.4 nm B_4C coating was verified only on the test grating as discussed in Section 4.1 and not on the actual gratings G1, G2, to avoid the risk of compromising the cleanliness and structure of the coated grating surface. Given that the topography and surface quality of the un-coated gratings G1, G2 was found to be very similar to the test grating, we anticipate that the same will be true after B_4C coating. Therefore, we consider the results presented in Section 4.1 for the B_4C-coated test grating to also be representative of the B_4C-coated gratings G1, G2.

The diffraction efficiency of the B_4C-coated gratings G1, G2 was measured at ALS beamline 6.3.2, in the portion of the photon energy range of relevance to SXR that is accessible by the beamline. Fig. 8 shows plots of diffraction efficiency vs. grating rotation angle ϕ (between incident photon beam and grating surface) at various SXR photon energies, for each of the G1, G2 gratings. The grating rotation angles ϕ where diffraction orders (peaks) are expected to appear, are governed by the equation:

$$m\lambda = 2\, d\, \cos\theta \sin(\varphi_0 - \varphi) \qquad (2)$$

where m is the grating order (0, ±1, ±2, … etc), λ is the wavelength, d is the grating period, 2θ = 178.4 degrees is the angle between the incident photon beam and the detector, and φ_0 = 0.8

degrees is the 0^{th} order ($m = 0$) angle. This equation is a variation of the standard grating equation for a "constant deviation" monochromator. The SXR monochromator utilizes the 1^{st} negative grating diffraction order ($m = -1$). Fig. 9 shows measured peak diffraction efficiency of the $m = +1$ order vs. photon energy for the G1 and G2 gratings. In measuring the diffraction efficiency over a photon energy range, the positive first order was chosen because of the larger angular width in comparison with the negative first order. As is also demonstrated in Fig. 8, positive orders have larger angular width because they correspond to shallower grazing incidence angles, where the diffracted beam is wider due to the grating demagnification properties, compared to the negative orders. In the geometry of fixed θ, the efficiency of the positive and negative first orders is equivalent according to the reciprocity theorem. It should be noted that scattering from a 1200 lines/mm monochromator grating at beamline 6.3.2, which was used in these measurements, introduces a small error which leads to under-estimation of the as-measured peak diffraction efficiency data shown in Fig. 9. Although this error is photon energy-dependent and would be impossible to determine separately for each photon energy, we attempted to apply a correction to the as-measured data based on estimates determined with the following method: we selected a set of filters already installed at beamline 6.3.2 (Cr, Ti, Cu) with absorption edges within the energy range of the measurements in Fig. 9. For each of these filters, we performed a scan of the transmitted signal vs. photon energy across the absorption edge. The normalized results are shown in Fig. 10 and are compared with calculations. The difference between the calculation and the measured results in the energy region above the absorption edge represents the error (percentage) introduced in that energy region due to scattering from the beamline 6.3.2 monochromator. These experimentally determined errors were extrapolated and used to correct the measured data shown in Fig. 9. The corrected data in Fig. 9 were fitted to theoretical

calculations using the GSolver© Diffraction Grating Analysis Program[21], to estimate the grating groove depth and line width parameters for each of the G1, G2 gratings. As is shown in Fig. 9, the fitted grating parameters are in remarkable agreement with the specified values for each grating, given in Table 1. The theoretically-calculated diffraction efficiencies in Fig. 9 are also in excellent agreement with the experimental results, which verifies the feasibility and successful operation of these B_4C-coated diffraction gratings in the 500-2000 eV photon energy region of the SXR beamline.

The un-ruled portion of the SXR gratings, which consists of a polished Si substrate coated with 37.4 nm of B_4C and is expected to be identical to the M1, M2 and M3 mirrors described in Section 3, was also measured at beamline 6.3.2. Fig. 11 shows the results of the reflectance vs. photon energy scans, performed at 0.8 degrees grazing angle of incidence, which is the nominal angle of operation for the SXR mirrors as shown in Table 1. The measurements in Fig. 11 are consistent with a calculated model using the IMD program[22]. The model uses as input parameters the experimentally determined thickness (from Fig. 4) and the optical properties (from Ref. 19) of the B_4C coating, and AFM-measured surface roughness values of the Si substrate and B_4C coating. The reflective performance shown in Fig. 11 should be considered as representative of the performance of the M1, M2 and M3 mirrors at the SXR beamline, given that all mirror and grating substrates were polished by the same vendor and have identical B_4C coatings.

5. Conclusions

We have successfully developed, fabricated and calibrated the mirrors and gratings for the SXR beamline at the LCLS FEL. Each element consists of a Si substrate coated with a B_4C thin film that ensures high reflective performance and FEL damage resistance. Thickness uniformity better than 0.14 nm rms was achieved for all B_4C coatings in the clear aperture region of each mirror

and grating. The B_4C coating uniformity, combined with low substrate figure errors, ensure the coherent wavefront preservation of the LCLS FEL beam. The diffraction efficiency of B_4C-coated gratings was demonstrated and calibrated for operation in the 500 – 2,000 eV photon energy region.

Acknowledgements

The authors are thankful to Jay Ayers (LLNL) for assistance with the design of the coating fixtures and Sunling Yang (LBNL) for assistance with the measurements at ALS beamline 6.3.2. We are grateful to Helge Thiess and Holger Lasser (Carl Zeiss Laser Optics, Oberkochen, Germany) for figure measurement results. Financial support for Mónica Fernández-Perea was provided in part by Ministerio de Educacion y Ciencia, Programa Nacional de Movilidad de Recursos Humanos del Plan nacional de I+D+I 2008-2011. This work was performed under the auspices of the U.S. Department of Energy by Lawrence Livermore National Laboratory under Contract No. DE-AC52-07NA27344, and by the University of California Lawrence Berkeley National Laboratory under Contract No. DE-AC03-76F00098. The Advanced Light Source is supported by the Director, Office of Science, Office of Basic Energy Sciences, of the U.S. Department of Energy under Contract No. DE-AC02-05CH11231. This work was carried out in support the SXR Instrument at the Linac Coherent Light Source (LCLS), a division of SLAC National Accelerator Laboratory and an Office of Science user facility operated by Stanford University for the U.S. Department of Energy. The SXR Instrument is funded by a consortium whose membership includes the LCLS, Stanford University through the Stanford Institute for Materials Energy Sciences (SIMES), Lawrence Berkeley National Laboratory (LBNL), University of Hamburg through the BMBF priority program FSP 301, and the Center for Free Electron Laser Science (CFEL).

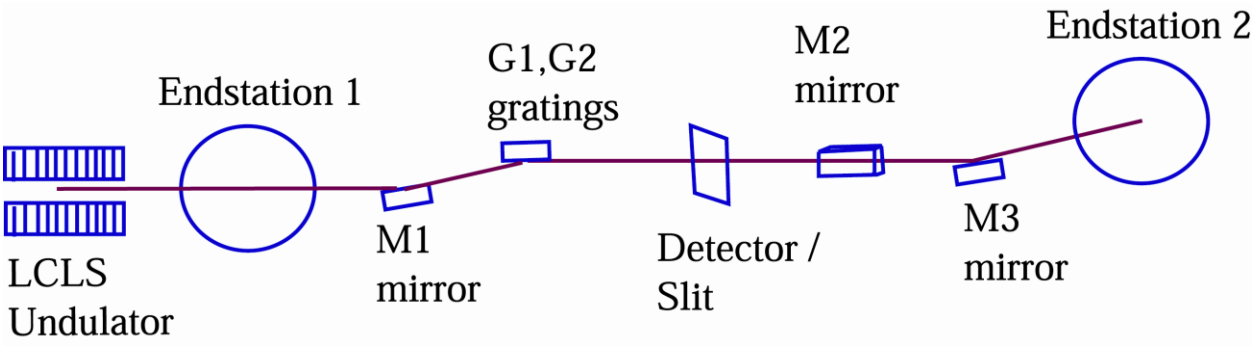

Fig. 1: Layout of the SXR beamline and its optical elements

	Type	Dimensions ($L \times W \times H$) (mm^3)	Clear Aperture (mm^2)	Grazing incidence angle(°)
M1	Spherical mirror	300 x 110 x 75	205 x 88	0.8
G1, G2	Plane VLS Gratings G1 = 100 lines /mm Z_0=28 $\pm$ 2 nm X_0=2.8 $\pm$ 0.2 μm G2 = 200 lines /mm Z_0=13 $\pm$ 1 nm X_0=2.05 $\pm$ 0.1 μm	220 x 50 x 23	180 x 34	1.44-0.97
M2	Plane mirror*	400 x 25 x 25	205 x 10	0.8
M3	Plane mirror*	400 x 25 x 25	150 x 10	0.8

Table 1: Summary of characteristics of the SXR beamline optics. The substrate material is single-crystal Si and the reflective coating is B_4C for all optics. The specified groove depth (Z_0) and line width (X_0) is also shown for each of the monochromator gratings G1, G2.

* Mirrors M2 and M3 were plane during the metrology and coating work described in this manuscript. They were bent to an elliptical shape at a later time, for installation at the SXR beamline. For more details see Ref. **Error! Bookmark not defined.**.

Optic	Data type	Radius (m)	Slope error (µrad rms)	Figure error (nm rms)
M1	Specified	1,049±40 (spherical)	0.3	2
	Measured	1,071.7	≤ 0.14	1.7*
M2	Specified	>1,000 <-2,000	0.3	2
	Measured	-23,570	≤ 0.2	1.25*
M3	Specified	>1,000 <-2,000	0.3	2
	Measured	-35,840	≤ 0.15	0.42*

** Measured by Carl Zeiss Laser Optics.*

Table 2: Radius of curvature and surface slope measurements determined via long-trace profilometry and figure error measurements provided by the vendor are shown together with the specifications for the SXR M1, M2, and M3 mirror substrates. The spatial period range of the measurements extends from 1 mm to the clear aperture, defined in Table 1 for each mirror.

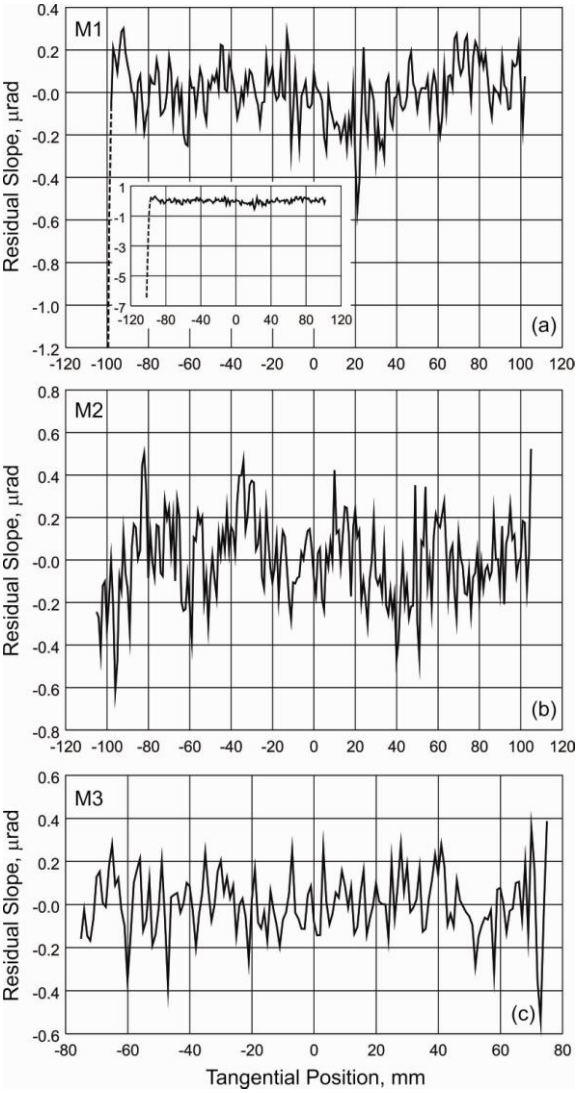

Fig. 2: Residual slope traces of the SXR (a) M1, (b) M2, and (c) M3 mirror substrates as they were measured with the long-trace profiler LTP-II. The residual slope traces were obtained by detrending the measured slope traces with the best-fit cylindrical shapes. For the M2 and M3 substrates, the fitting and detrending were made over the entire clear aperture, specified in Table 1 for each mirror. For the M1 substrate, the fitting was made over the surface area less by 3 mm than the specified clear aperture. The dashed lines in the plot (a) and the inset depict the excluded portion of the slope trace.

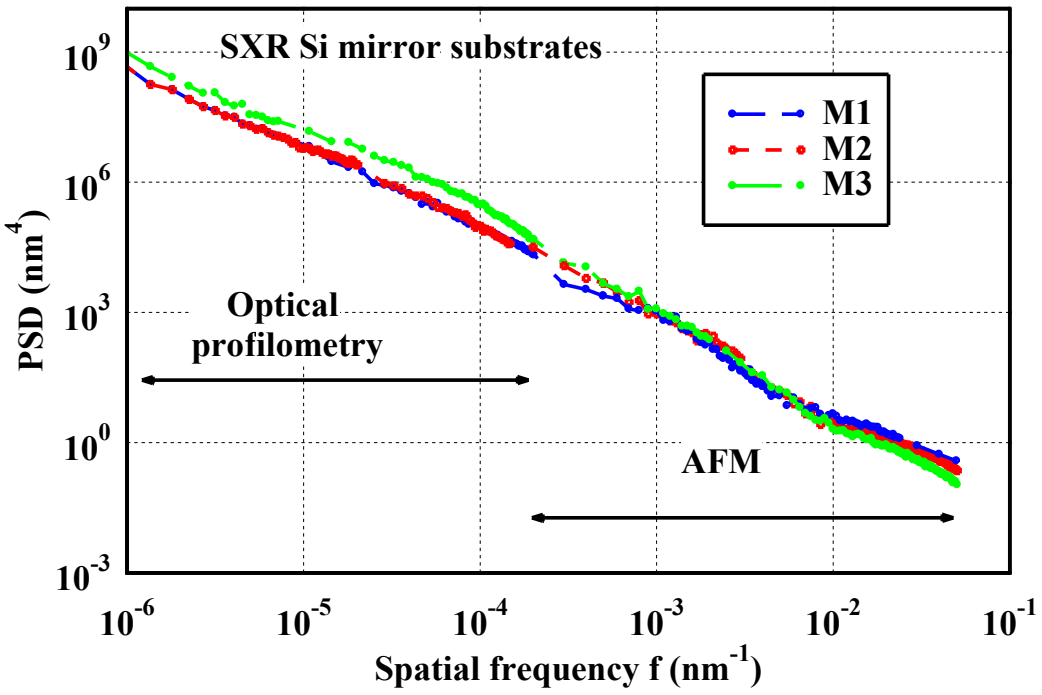

Fig. 3: PSD curves are plotted in the MSFR and HSFR ranges for each of the SXR mirror substrates. Each PSD curve is derived from precision surface metrology data averaged from measurements on 2 locations.

	M1	M2	M3	Specification
HSFR (nm rms)	0.13	0.13	0.13	**0.4**
MSFR (nm rms)	0.17	0.19	0.29	**0.4**

Table 3: Precision surface metrology results for the HSFR and MSFR on SXR Si mirror substrates M1, M2 and M3 are shown, together with the specifications. The spatial frequency ranges corresponding to MSFR and HSFR are defined as follows: MSFR: from 10^{-6} nm^{-1} to 5×10^{-4} nm^{-1}. HSFR: from 5×10^{-4} nm^{-1} to 5×10^{-2} nm^{-1}.

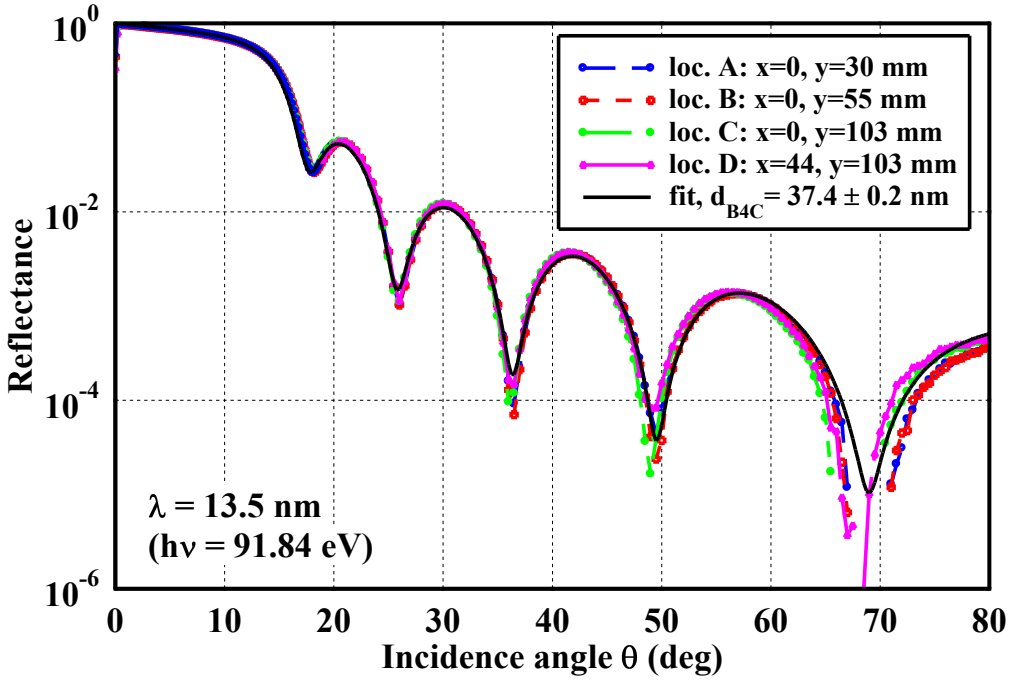

Fig. 4: Reflectance vs. incidence angle measurements on a B_4C-coated test Si substrate, performed as part of the thickness uniformity optimization on the SXR M1 mirror. The *y*-direction was defined to coincide with the center line of the mirror in the tangential direction, with *x*, *y* = 0 being the center of the mirror. Given that coating thickness variation is symmetric around the center of the mirror, only data for positive *y* values are plotted above. The best fit to the reflectance data plotted above was produced with a B_4C coating thickness d_{B4C} = 37.4 nm. B_4C optical constants from the CXRO Atomic Data Tables[23] and from recently determined experimental values[19] at 13.5 nm wavelength produced the same value for the fitted B_4C coating thickness.

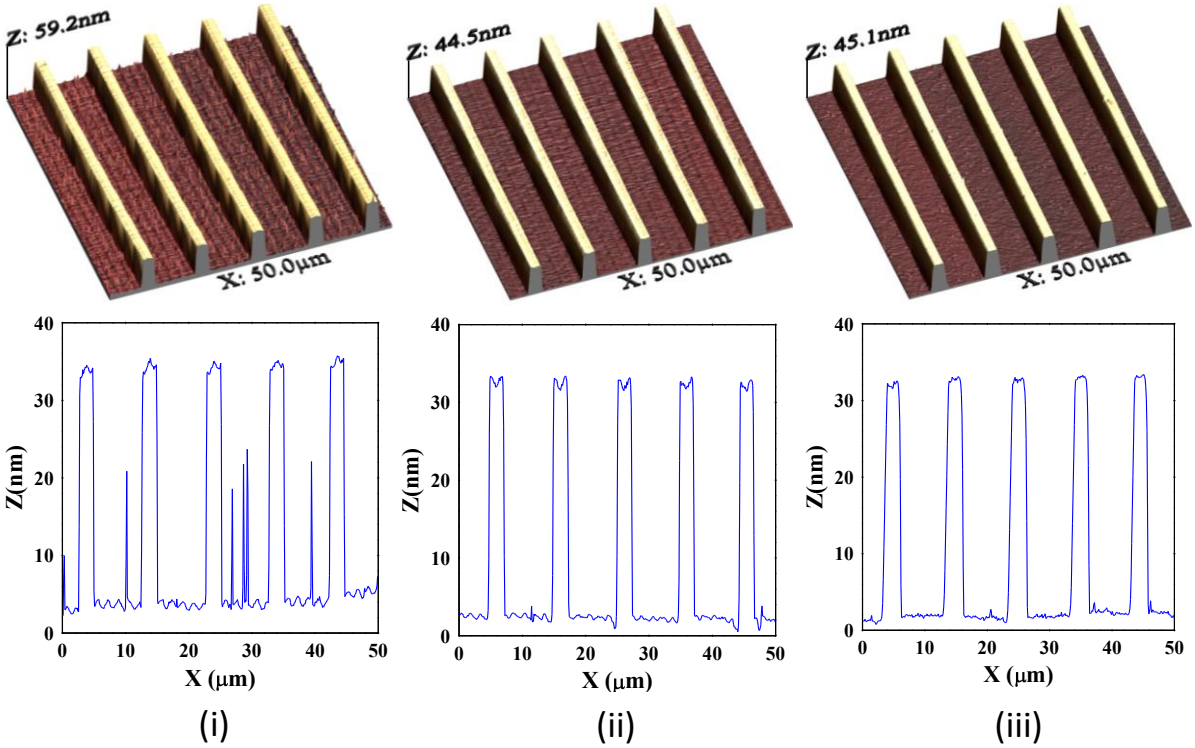

Fig. 5: 3-dimensional, 50×50 μm^2 AFM images and representative 1-dimensional line scans, obtained on the 100 lines/mm test grating (i) as-received from the manufacturer, (ii) after cleaning and (iii) after coating with a 37.4 nm – thick B_4C coating.

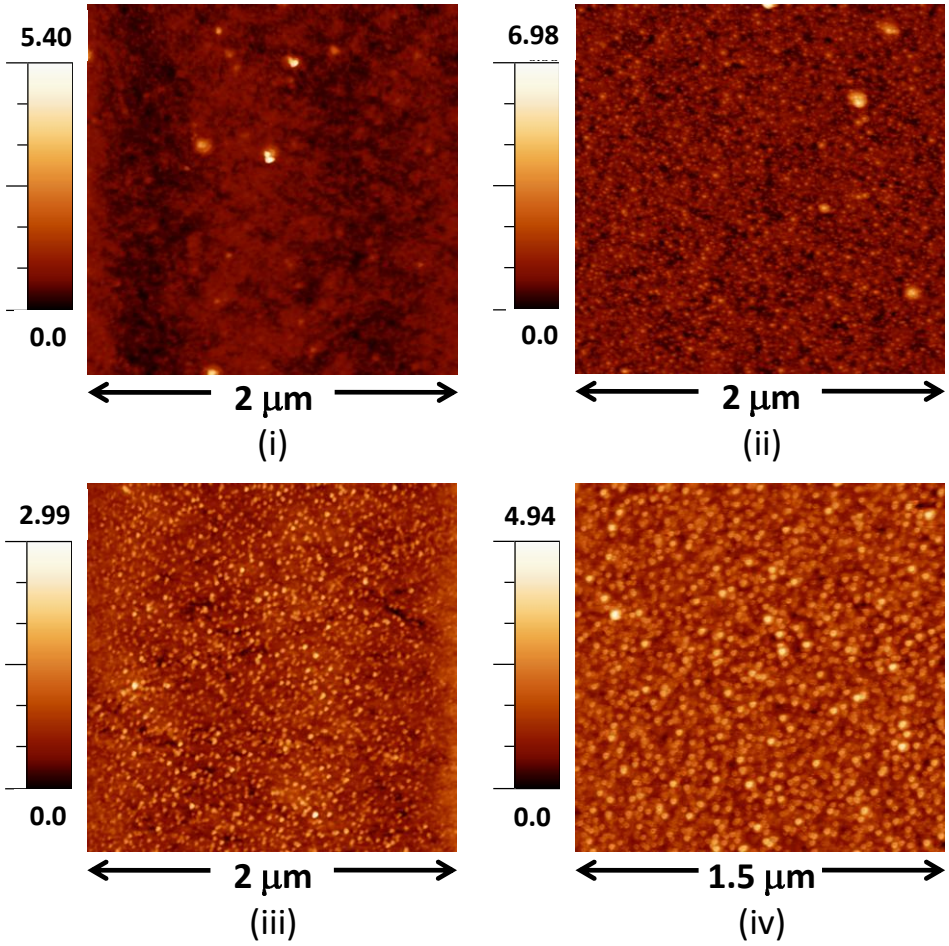

Fig. 6: AFM images obtained from the 100 lines/mm test grating after cleaning (i) 2×2 μm^2, groove area, (ii) 2×2 μm^2 groove area after B_4C coating, (iii) 2×2 μm^2 line area, (iv) 1.5×1.5 μm^2 line area after B_4C coating. The B_4C coating thickness is 37.4 nm. The units on the scale bars on the left of each AFM image are nm.

sample area	**description**	**size (μm^2)**	**HSFR (nm rms)**
groove	as-received	5×5	0.73
groove	"	2×2	0.48
line	"	2×2	0.20
groove	after cleaning	2×2	0.22
line	"	2×2	0.27
groove	after cleaning and coating with B_4C	2×2	0.41
line	"	1.5×1.5	0.49

Table 3: Measured HSFR values of the 100 lines/mm test grating, obtained from two-dimensional power spectral density analysis of AFM data at different locations and cleaning/coating stages. HSFR is computed in the spatial frequency range 10^{-3} nm^{-1} to 5×10^{-2} nm^{-1}.

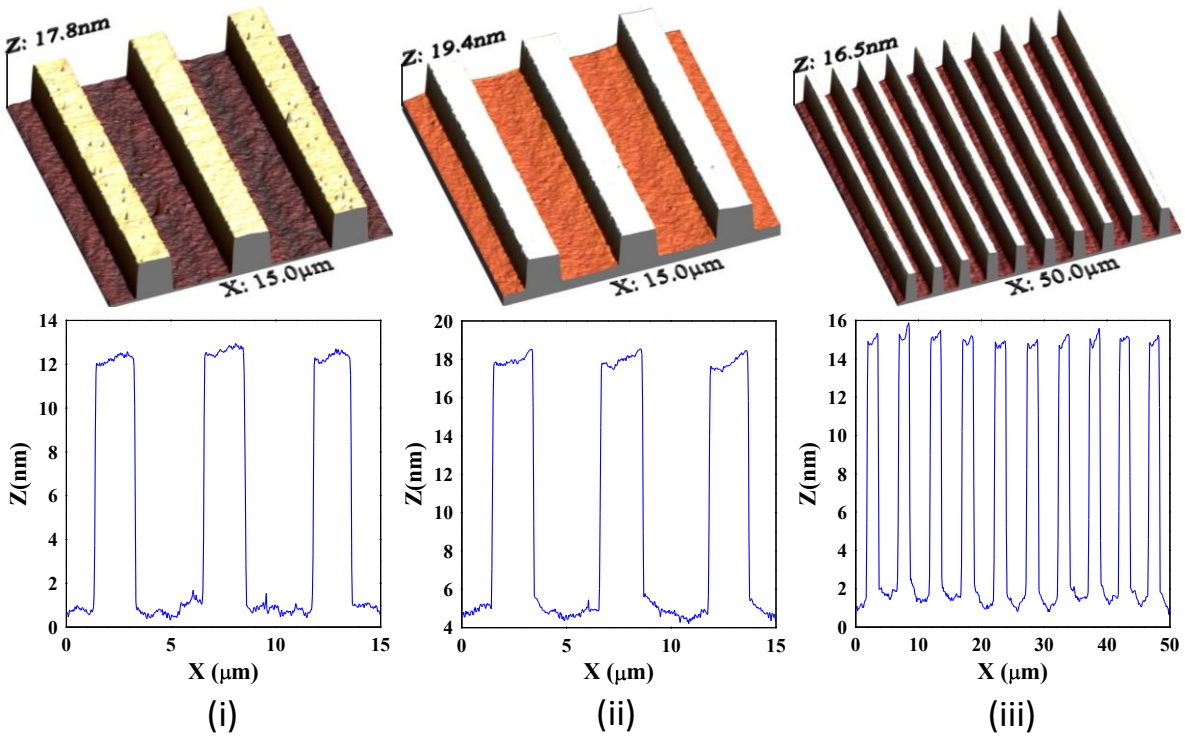

Fig. 7: 3-dimensional AFM images and representative 1-dimensional line scans, obtained on the 200 lines/mm G2 grating (i) 15×15 μm^2, as-received from the manufacturer, (ii) 15×15 μm^2, after cleaning, and (iii) 50×50 μm^2, after cleaning.

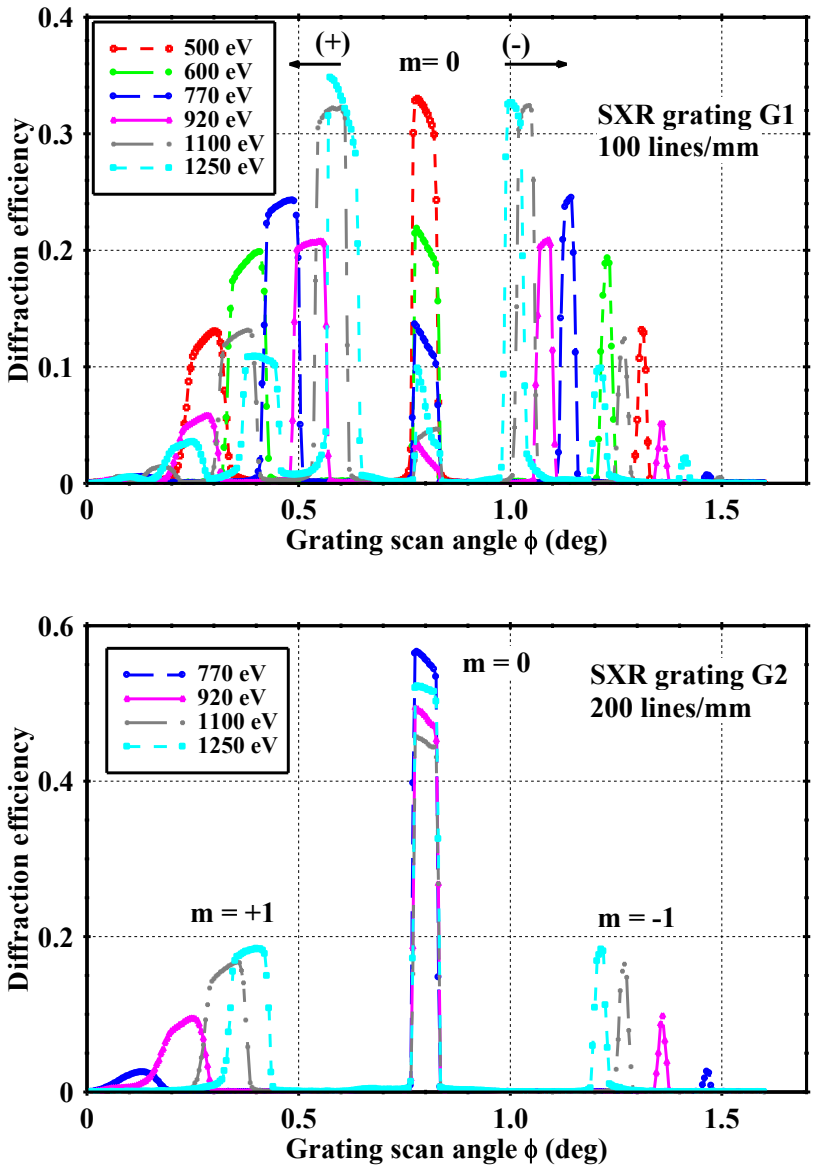

Fig. 8: Measured diffraction efficiency vs. grating rotation angle ϕ is plotted for SXR grating G1 (top) and G2 (bottom) at different photon energies. The detector angle was fixed at 178.4 degrees from the incident photon beam, which is the designed angle of operation at the SXR beamline. In the top plot, the arrows point to the direction of the positive (+) and negative (-) grating diffraction orders.

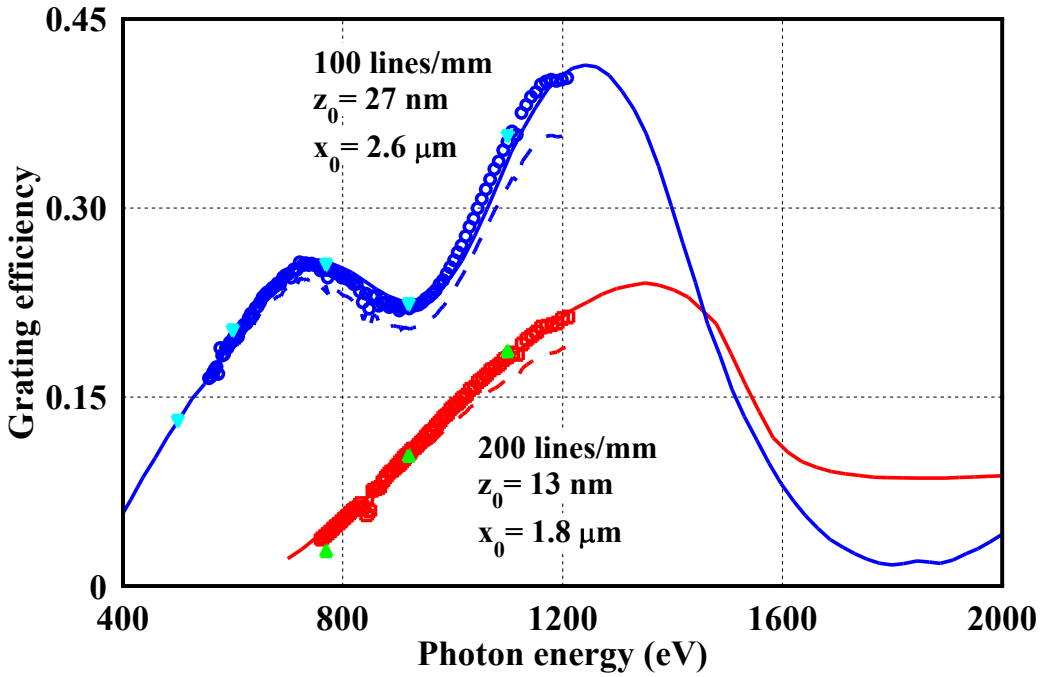

Fig. 9: Measured diffraction efficiencies (1st positive order) of the SXR gratings G1 and G2 are shown as data points. The dip-like feature near 853 eV is attributed to the Ni $L_{2,3}$ absorption edge and is likely due to a Ni-coated mirror at ALS beamline 6.3.2[16]. The isolated data points (triangles) correspond to measured data from Fig. 8. A correction has been applied to all measured data points, to account for the scattering from the ALS beamline 6.3.2. monochromator. Measured diffraction efficiencies before applying the scattering correction are also shown as dash lines. The corrected measured results are fitted to calculations (solid lines) using the GSolver© Diffraction Grating Analysis Program[21]. The fitted values for the groove depth (z_0) and line width (x_0) are also shown for each grating, and are in excellent agreement with the specified values given in Table 1.

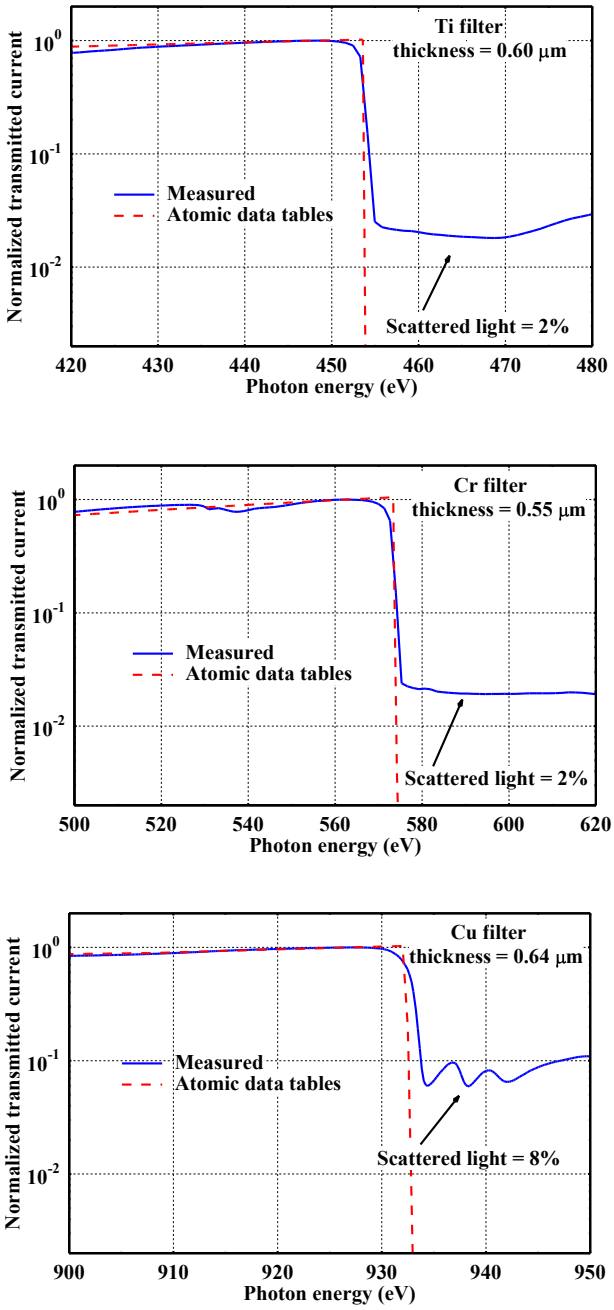

Fig. 10: The normalized transmitted current is plotted vs. photon energy across the $L_{2,3}$ absorption edge of a Ti filter (top), Cr filter (middle) and Cu filter (bottom). The scans were performed at ALS beamline 6.3.2, with the 1200 lines/mm monochromator grating. These results were compared with theoretical calculations from the CXRO Atomic Data Tables[23] and were used to estimate the amount of scattered light from the 1200 lines/mm monochromator grating.

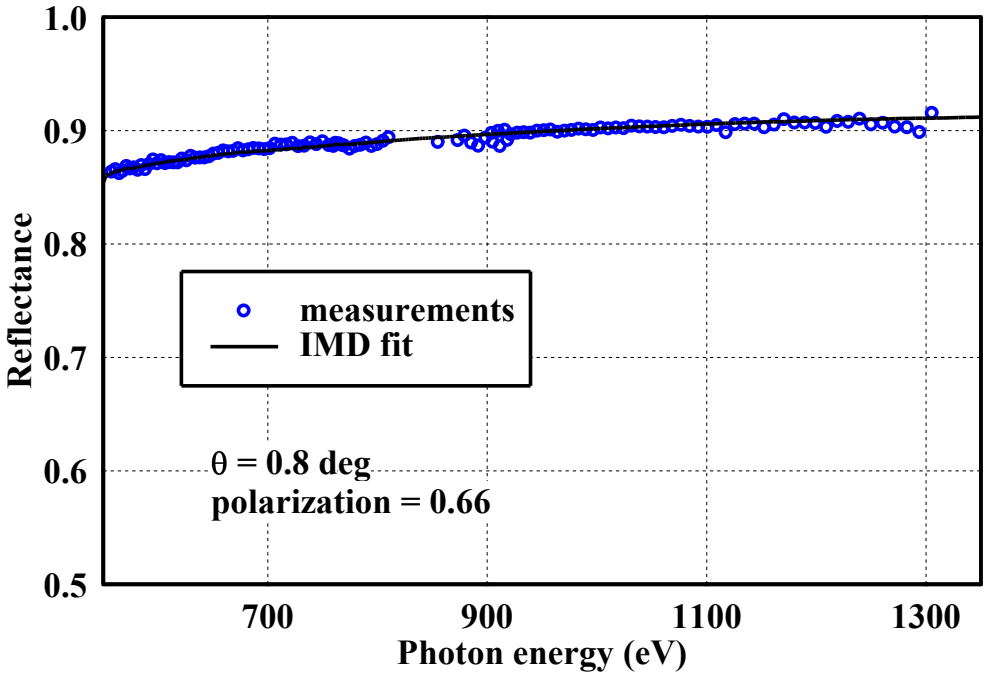

Fig. 11: Measured reflectance vs. photon energy at ALS beamline 6.3.2. of the un-ruled portion of the B_4C-coated SXR gratings G1, G2 and comparison to a calculated model using the IMD program[22]. Measurements were done at the SXR mirror incidence angle $\theta = 0.8$ deg. Polarization at beamline 6.3.2 is estimated to be about 0.66 in this photon energy range, with 1 corresponding to a fully s-polarized beam.

References

[1] For more details see the official LCLS Website at http://lcls.slac.stanford.edu/

[2] For more details see the official SXR beamline Website at https://slacportal.slac.stanford.edu/sites/lcls_public/instruments/SXR/Pages/default.aspx

[3] P. Heimann, O. Krupin, W. F. Schlotter, J. Turner, J. Krzywinski, F. Sorgenfrei, M. Messerschmidt, D. Bernstein, M. Holmes, N. Kelez, D. Nordlund, M. Fernandez-Perea, R. Soufli, W. Wurth and M. Rowen, "Linac Coherent Light Source Soft X-ray Materials Science Optical Design and Monochromator Commissioning", Rev. Sci. Instrum. **82**, 093104 (2011).

[4] M. Pivovaroff, R. M. Bionta, T. J. Mccarville, R. Soufli, P. M. Stefan, "Soft X-ray mirrors for the Linac Coherent Light Source", Proc. SPIE **6705**, 67050O (2007).

[5] R. Soufli, M. J. Pivovaroff, S. L. Baker, J. C. Robinson, E. M. Gullikson, T. J. McCarville, P. M. Stefan, A. L. Aquila, J. Ayers, M. A. McKernan, R. M. Bionta, "Development, characterization and experimental performance of x-ray optics for the LCLS free-electron laser" Proc. SPIE **7077,** 707716 (2008).

[6] T. J. McCarville, P. M. Stefan, B. Woods, R. M. Bionta, R. Soufli, M. J. Pivovaroff, "Opto-mechanical design considerations for the Linac Coherent Light Source X-ray mirror system", Proc. SPIE **7077,** 70770E (2008).

[7] A. Barty, R. Soufli, T. McCarville, S. L. Baker, M. J. Pivovaroff, P. Stefan and R. Bionta, "Predicting the coherent X-ray wavefront focal properties at the Linac Coherence Light Source (LCLS) X-ray free electron laser", Optics Express **17**, 15508-15519 (2009).

[8] N. Kelez, J. Bozek, Y.-D. Chuang, R. Duarte, D.E. Lee, W. McKinney, V. V. Yashchuk, S. Yuan, "*Design, Modeling, and Optimization of Precision Bent Refocus Optics – LCLS AMO KB Mirror Assembly*," Proc. of FEL2009, 546-549 (Liverpool, UK, 2009); http://accelconf.web.cern.ch/accelconf/FEL2009/papers/wepc20.pdf.

[9] S.P. Hau-Riege, R.A. London, R.M. Bionta, D. Ryutov, R. Soufli, S. Bajt, M.A. McKernan, S.L. Baker, J. Krzywinski, R. Sobierajski, R. Nietubyc, J. B. Pelka, M. Jurek, L. Juha, J. Chalupský, J. Cihelka, V. Hájková, A. Velyhan, J. Krása, J. Kuba, K. Tiedtke, S. Toleikis, H. Wabnitz, M. Bergh, C. Caleman, N. Timneanu, "Wavelength dependence of the damage threshold of inorganic materials under extreme-ultraviolet free-electron-laser irradiation", Appl. Phys. Lett. **95,** 111104 (2009).

[10] S.P. Hau-Riege, R.A. London, A.Graf, S. L. Baker, R. Soufli, R. Sobierajski, T. Burian, J. Chalupsky, L. Juha, J. Gaudin, J. Krzywinski, S. Moeller, M. Messerschmidt, J. Bozek, and Ch. Bostedt,"Interaction of low-Z inorganic solids with short x-ray pulses at the LCLS free-electron laser", Optics Express **18**, 23933-23938 (2010).

[11] J. L. Kirschman, E. E. Domning, W. R. McKinney, G. Y. Morrison, B. V. Smith, and V. V. Yashchuk, "Performance of the upgraded LTP-II at the ALS Optical Metrology Laboratory," Proc. SPIE **7077**, 70770A/1-12 (2008).

[12] V. V. Yashchuk, S. Barber, E. E. Domning, J. L. Kirschman, G. Y. Morrison, B. V. Smith, F. Siewert, T. Zeschke, R. Geckeler, A. Just, "Sub-microradian Surface Slope Metrology with the ALS Developmental Long Trace Profiler," Nucl. Instr. and Meth. A **616**, 212-223 (2010).

[13] R. Soufli, S. L. Baker, D. L. Windt, J. C. Robinson, E. M. Gullikson, W. A. Podgorski, L. Golub, "Atomic force microscopy characterization of Zerodur mirror substrates for the extreme

ultraviolet telescopes aboard NASA's Solar Dynamics Observatory", Appl. Opt. **46**, 3156-3163 (2007).

[14] D. L. Windt, "topo - surface topography analysis", available at http://www.rxollc.com/idl/index.html

[15] R. Soufli, R. M. Hudyma, E. Spiller, E. M. Gullikson, M. A. Schmidt, J. C. Robinson, S. L. Baker, C. C. Walton, and J. S. Taylor "Sub-diffraction-limited multilayer coatings for the 0.3 numerical aperture micro-exposure tool for extreme ultraviolet lithography", Appl. Opt. **46**, 3736-3746 (2007).

[16] J. H. Underwood, E. M. Gullikson, "High-resolution, high-flux, user friendly VLS beamline at the ALS for the 50-1300 eV energy region," J.Electr. Spectr. Rel. Phenom. **92**, 265-272 (1998).

[17] E. M. Gullikson, S. Mrowka, B. B. Kaufmann, "Recent developments in EUV reflectometry at the Advanced Light Source," in *Emerging Lithographic Technologies*., V. E. A. Dobisz ed., Proc. SPIE **4343**, 363-373 (2001).

[18] R. Soufli, S. L. Baker, J. C. Robinson, E. M. Gullikson, T. J. McCarville, M. J. Pivovaroff, P. Stefan, S. P. Hau-Riege, R. Bionta, "Morphology, microstructure, stress and damage properties of thin film coatings for the LCLS x-ray mirrors", Proc. SPIE **7361,** 73610U (2009).

[19] R. Soufli, A. L. Aquila, F. Salmassi, M. Fernández-Perea, E. M. Gullikson, "Optical constants of magnetron sputtered boron carbide thin films from photoabsorption data in the range 30 to 770 eV", Appl. Opt. **47**, 4633-4639 (2008).

[20] I. Horcas, R. Fernandez, J.M. Gomez-Rodriguez, J. Colchero, J. Gomez-Herrero, and A.M. Baro, Rev. Sci. Instrum **78**, 013705 (2007).

[21] See http://www.gsolver.com/ for a detailed description of this program.

[22] D. L. Windt, "IMD: Software for modeling the optical properties of multilayer films," Computers in Physics **12**, 360–370, 1998. Available at http://www.rxollc.com/idl/index.html.

[23] B.L. Henke, E.M. Gullikson, and J.C. Davis, "X-ray interactions: photoabsorption, scattering, transmittance, and reflection at E=50-30000 eV, Z=1-92", Atomic Data and Nuclear Data Tables **54** , 181-342 (1993). Database is currently maintained by E. M. Gullikson at CXRO, available at http://henke.lbl.gov/optical_constants/